science.sciencemag.org/cgi/content/full/science.aay5820/DC1

Supplementary Materials for

Satellite testing of a gravitationally induced quantum decoherence model

Ping Xu*, Yiqiu Ma*, Ji-Gang Ren*, Hai-Lin Yong, Timothy C. Ralph, Sheng-Kai Liao, Juan Yin, Wei-Yue Liu, Wen-Qi Cai, Xuan Han, Hui-Nan Wu, Wei-Yang Wang, Feng-Zhi Li, Meng Yang, Feng-Li Lin, Li Li, Nai-Le Liu, Yu-Ao Chen, Chao-Yang Lu, Yanbei Chen, Jingyun Fan†, Cheng-Zhi Peng†, Jian-Wei Pan†

*These authors contributed equally to this work.
†Corresponding author. E-mail: fanjy@ustc.edu.cn (J.F.); pcz@ustc.edu.cn (C.-Z.P.); pan@ustc.edu.cn (J.-W.P.)

Published 19 September 2019 on *Science* First Release
DOI: 10.1126/science.aay5820

This PDF file includes:

Materials and Methods

Parameter Δ

The parameter which controls the strength of the varying commutation relation between event mode operators (and hence the decorrelation of entanglement) is Δ.

Δ parametrizes the difference between the globally defined detection time t_d and a locally defined time τ:

$$\Delta \;=\; t_d - \tau(t, t_d). \tag{1}$$

The parameter $\tau(t, t_d)$ records the propagation time between the detection time, t_d, and t, as incrementally measured by a set of local observers along the light path of this particular mode, i.e.

$$\tau(t, t_d) = \int_t^{t_d} ds, \tag{2}$$

where ds is the propagation time across an incremental local frame. It is required that these local frames are all at rest with respect to the frame of reference in which the detector is stationary. This uniquely defines a locally measured time along the propagation path.

The other component of Δ is the globally defined detection time, t_d. A natural choice is to take the global time reference to be that of an asymptotically flat region of space-time. For example, if we are considering a situation described by the Schwarzschild metric (as for Earth) then t_d would be the Schwarzschild time coordinate (far-away time).

In ref. (*13*) the ground to satellite situation was considered and the expression for $\Delta_t = \Delta_2 - \Delta_1$ was derived, where Δ_1 is for the photon trajectory which stays on the ground and Δ_2 is for the photon that travels to the satellite. With a particular choice of the time origin we have $\Delta_1 \approx 0$ and:

$$\Delta_t \approx \int_{r_e}^{r_e+h} \frac{M}{r}(1 + \frac{2M}{r} + \frac{r_e^2 \tan^2(90-\theta)}{r^2})^{1/2} dr, \tag{3}$$

where r_e is Earth radius, h is the satellite height, m is the mass of the Earth expressed in units of length and θ is the altitude angle. The theory comparisons in the main text are based on eq. (3).

The global time reference, t_d, in the previous calculation (and the original proposal) was taken to be that of an asymptotically flat region of space-time. The logic of this was to compare propagation in flat-space to that in curvature. However, this approach has some ambiguities when considering more general situations, and also arguably does not seem to fit so well with the local nature of general relativity.

Another possibility is that the global time reference should be the proper time of the detector. This removes possible ambiguities and provides a local nature to the theory. In this case, Δ now parameterizes the difference between the detection time, t'_d, measured at the detector and the time measured by local observers along the path $\tau(t, t_d)$. This difference is the effective curvature effect observable from the vantage point of the detector (as opposed to that observable by a far-away observer). The two definitions coincide if the detections are carried out far from the

source of curvature, but lead to more stringent requirements for the observation of decoherence from sources and detectors within the gravitational field.

Suppose for simplicity that the metric, $g_{\alpha\beta}$ is diagonal and that the time co-ordinate of the metric corresponds to a far-away clock in asymptotically flat-space. Let us also suppose that the detector and far away clocks are synchronised at the source emission time, $t = t' = 0$. We can calculate t_d for a light-like (null) geodesic as

$$t_d = \int_{x_s}^{x_d} \sqrt{\frac{g_{ii}}{-g_{00}}} dx_i \tag{4}$$

where x_s and x_d are the positions of the source and detectors respectively, g_{00} is the time component of the metric, g_{ii} is the spacial component of the metric in the incremental direction dx_i, and the integral is along the path between source and detector. Then the proper time told by the detector is given by

$$t'_d = \sqrt{-g_{00}|_{x_i=x_d}} t_d \tag{5}$$

Applying this to the situation considered in the main text the expression for Δ_t becomes:

$$\Delta_t = \int_{r_e}^{r_e+h} (\frac{M}{r} - \frac{M}{r_e+h})(1 + \frac{2M}{r} + \frac{r_e^2 \tan^2(90-\theta)}{r^2})^{1/2} dr \tag{6}$$

The plot in Fig. S1 demonstrates the stricter requirements predicted to be needed in order to see decoherence with this definition for Δ_t. Now the decoherence factor $D \approx \exp(-0.5\Delta_t^2/d_t^2)$ is between 0.96 to 0.98 ($40^\circ < \theta < 60^\circ$) for 0.07 mm pulses distributed to a height of 500 km.

The difference between decorrelation ($D \sim 0.96$) due to the weaker decoherence effect and no-decorrelation ($D = 1$) is about 0.04. Then the experimental result is meaningful only if the noise is at most a fraction of the difference. We estimate it will take about 300 satellite passes, which requires at least three years, to have enough experimental data such that the relative 1-standard deviation is 1/3 of the difference, assuming a very stable experimental condition. Note that, for the current experimental configuration (Low Earth Orbit for *Micius*) the time needed to complete such a meaningful experimental study of the weaker decoherence effect (3 years) is far beyond the rest of *Micius* lifetime. We are planning to launch a MEO (Middle Earth Orbit)-to-GEO (Geostationary Transfer Orbit) quantum satellite around the year of 2024, with an altitude between 10,000 km and 36,000 km. Studying the interplay between quantum physics and gravity is listed as one of the main scientific missions. With this new satellite, the decorrelation factor due to the weaker decoherence effect is estimated to be close to zero (at the order of $D \sim 10^{-100}$), which can be easily verified.

Spectrum of the photons

The quantum state produced in the spontaneous parametric down-conversion (SPDC) process in the main text, in the weak pump limit, may be described by:

$$\begin{aligned} |\Psi\rangle_{12} = &|vac\rangle + \sqrt{\frac{p}{2}} \left(\hat{a}^\dagger_{1\mathrm{H}}\hat{a}^\dagger_{2\mathrm{H}} + \hat{a}^\dagger_{1\mathrm{V}}\hat{a}^\dagger_{2\mathrm{V}}\right)|vac\rangle \\ &+ \frac{p}{4}\left(\hat{a}^\dagger_{1\mathrm{H}}\hat{a}^\dagger_{2\mathrm{H}} + \hat{a}^\dagger_{1\mathrm{V}}\hat{a}^\dagger_{2\mathrm{V}}\right)^2 |vac\rangle\,, \end{aligned} \tag{7}$$

where *p* is the generation probability of one photon pair per pump pulse, $|vac\rangle$ is the vacuum state, and $\hat{a}^{\dagger}$ is the creation operator with subscripts 1 and 2 for paths 1 and 2 and H and V for the horizontal and vertical polarization states, respectively. We pass photons in path 2 through a polarization beam splitter (PBS) (Fig. S2A). The simultaneous detections of single photons at both ports of the PBS in path 2 herald the presence of two-photon state $|H,V\rangle_1$ in path 1. We feed the two-photon state $|H,V\rangle_1$ to a Hong-Ou-Mandel (HOM) interferometer. The first PBS in the interferometer of path 1 separates the two photons into two arms and the second PBS recombines them. The half-wave plates (HWPs) transform the polarization states to $|D\rangle = (|H\rangle + |V\rangle)/\sqrt{2}$ in both arms. We project the two outputs of the second PBS into $|D\rangle$ state before detection. By varying the relative delay between the two arms of the interferometer, the four-fold coincidence measurement (Fig. S2B) exhibits the Hong-Ou-Mandel dip.

Assuming the spectrum of entangled single photons is Gaussian (eq. (22) in ref. (*12*)),

$$H(\Omega) = \sqrt{\frac{\sqrt{2}d_{\mathrm{t}}}{\sqrt{\pi}}} e^{-(\Omega-\Omega_0)^2 {d_{\mathrm{t}}}^2}, \tag{8}$$

by applying the inverse Fourier transform $G(t) = F^{-1}\left(|H(\Omega)|^2\right)$, the autocorrelation function is given by $g(t) = G(t)/G(0) = e^{-\frac{t^2}{8d_{\mathrm{t}}}}$. Note that the coincidence gate width is 3 ns in our experiment, which is much longer than the correlation time of single photons, the coincidence counting rate in the HOM measurement is given by

$$N_{\mathrm{c}}(\delta t) \propto 1 - \frac{\int_{-\infty}^{\infty} g(t)\, g(t-2\delta t)\, dt}{\int_{-\infty}^{\infty} g^2(t)\, dt} = 1 - e^{-\frac{\delta t^2}{4{d_{\mathrm{t}}}^2}}, \tag{9}$$

where δt is the path imbalance $c\delta t$ in the HOM interferometer. Fitting eq. (9) to the experimental data (Fig. S2B), we obtain d_{t} = 0.07 mm.

Figure S3 depicts the calculated two-photon (amplitude) joint spectrum of photon pairs created in SPDC under the experimental condition and passing through Gaussian spectral filters (*32*), $A_\lambda(\lambda_1, \lambda_2)$, where λ_1 (ω_1) is the wavelength (frequency) of photons in path 1 (signal photons) and λ_2 (ω_2) is the wavelength (frequency) of photons in path 2 (idler photons). By performing the Schmidt decomposition to factorize the joint spectrum function (*33*):

$$A(\omega_1, \omega_2) = \sum_n \sqrt{\chi_n}\psi_n(\omega_1)\,\phi_n(\omega_2), \tag{10}$$

where

$$\begin{aligned} \sum_k K_1(\omega_{1i}, \omega_{1k})\psi_n(\omega_{1k}) &= \chi_n \psi_n(\omega_1), \\ \sum_k K_2(\omega_{2j}, \omega_{2k})\phi_n(\omega_{2k}) &= \chi_n \phi_n(\omega_2), \end{aligned} \tag{11}$$

with

$$K_1(\omega_{1i},\omega_{1k}) = \sum_j A(\omega_{1i},\omega_{2j})A^*(\omega_{1k},\omega_{2j}),$$
$$K_2(\omega_{2j},\omega_{2k}) = \sum_i A(\omega_{1i},\omega_{2j})A^*(\omega_{1i},\omega_{2k}). \quad (12)$$

We have χ_1 = 0.92 (Fig. S3), indicating that the pairs of photons are produced dominantly in a single eigen mode in our experiment. Correspondingly, from the eigen mode ψ_1 (ω_1), we estimate $d_{\rm t} \sim 0.06$ mm, which is consistent with the result obtained from the HOM measurement.

Spacetime analysis

As shown in Fig.1 of the main text, a pair of photons created in the BIBO via the SPDC process crystal interfere at a PBS. We take the time for the entangled pairs of photon exiting the PBS as the origin of the (vertical) time axis in Fig. S4B. As shown in Fig. S4A, the time elapsed (t_1) for entangled single photons in path 1 contains: 5 ns, for propagation in the lab; 90 ns, for fiber link from lab to the transmitter; 12 ns, latency inside the transmitter; 4 to 6 ns due to the atmospheric refraction; $t_{\rm vac}$, photon propagation time from ground station to satellite in vacuum; 7 ns, latency in the telescope at the satellite.

The time elapsed (t_2) for entangled single photons in path 2 includes: 16 ns, latency due to free space and fiber propagation; 65 ns, latency due to detection electronics including TDC; 20 ns for the spatial separation between TDC and the transmitter at the ground station; $t_{\rm vac}$, photon propagation time from ground station to satellite in vacuum.

So we have the time difference $\delta t = t_1 - t_2$, which is about 18 - 20 ns. Then events M1 and M2 are separated time-like.

As shown in Fig. S5, by adding a piece of 1 km optical fiber (about 5 μs) in path 2, we have the time difference, $\delta t = t_1 - t_2 - 5\mu s$, which is about -5 μs. Then events M1 and M2 are separated space-like.

Two photon-correlation measurement

In the experiment a Ti:Sapphire laser was used to deliver laser pulses at the wavelength of 780 nm periodically at a repetition period of $t_p = 12.5$ ns. Each optical pulse was assigned an experimental trial, in which $\sim 2\%$ of the laser pulse energy was picked up to produce a faint coherent laser pulse at a later stage. The rest of the laser pulse was up-converted to the wavelength of 390 nm to drive the spontaneous parametric down-conversion (SPDC) process which generates polarization-entangled pairs (Fig. 1B), $|\Phi^+\rangle_{12} = (|{\rm H}\rangle_1 |{\rm H}\rangle_2 + |{\rm V}\rangle_1 |{\rm V}\rangle_2)/\sqrt{2}$ at 780 nm wavelength, where H and V stand for horizontal and vertical polarization and 1 and 2 the spatial path degree-of-freedoms, respectively (*14*). The photons in path 2 are detected at the ground station while their entangled counterparts in path 1 are combined with the attenuated coherent laser pulses using a beam splitter, which transmits 98% of entangled single photons in path 1 and reflects 2% of coherent laser pulses. Prior to this combination, 2% of single photons in path 1 are dropped and detected in path $1'$ to monitor the system stability, and 2% of coherent laser pulses are dropped and detected in path 3 for two-photon coincidence measurement,

respectively. The output of the beam splitter now contains a train of single photons which are entangled with their twins in path 2 and a train of faint coherent laser pulses which are classically correlated with the laser pulses in path 3. The two trains of pulses which are relatively displaced by $0.5t_p(\sim 6$ ns) are sent to the satellite by a telescope with a diameter of 130 mm. The satellite has a telescope to receive this photon stream.

We insert a 3 nm bandpass filter before single photon detectors at satellite and in path $1'$ at the ground station, and 8 nm bandpass filters in paths 2 and 3 at the ground station, all of which are centered at 780 nm. After spectral filtering, the entangled photon pairs are nearly spectrally uncorrelated (with $\sim 90\%$ of two-photon spectral component in one mode, Supplementary Information 2.2) with each photon approximately in an eigen-pulse mode (*32,34*). These filters also block noise photons at other wavelength. We note that the spectrum of the coherent laser pulses from the Ti:Sapphire laser is ~ 6 nm. Passing the coherent laser pulses through a 3 nm bandpass filter is equivalent to attenuation without changing the classical correlation property. We employ silicon-based single photon avalanche diodes (SPAD) to detect single photons and record the detection signals by time-to-digital convertors (TDCs) at both ground station and satellite in the synchronized fashion. Aligning the TDC data between the ground station and the satellite yields two-photon coincidence events with a jitter (quantified by the half width at half maximum) of 1 ns (*14,35,36*). While photons pass through polarization analysis in both path 2 at ground station and satellite, we only use the information of arrival time regardless of the polarization status. To be specific, we denote the two-photon coincidence events between path 2 and satellite due to entangled photon pairs as $C_{\mathrm{exp,EPR}}(\theta)$ and between path 3 and satellite due to faint coherent laser pulses as $C_{\mathrm{exp,COH}}(\theta)$, both are functions of the altitude angle θ of the satellite (see Fig. 1A). The two-photon coincidence time window is set to 3 ns such that the single photon pulses are well discernible from the neighbors. We only perform the two-photon coincidence measurements at nights that have a clear sky condition and can only do one experimental run a night, i.e., we perform the two-photon coincidence measurements as the altitude angle θ changes from 40° to 60° one time a night as observed from the ground station.

In the satellite *Micius*-based quantum experiments, the recovery time (*37*) of the SPAD sets a limit to the rate of entangled photon pairs production at the ground station and the delivery of photons from the ground station to the satellite has a high loss. As a result, the detection rate of two-photon coincidence between satellite and ground station is low. To reduce the statistical error in the analysis, data grouping and statistical average are applied, see main text. In each run of the experiment, we group the two-photon coincidence events for every 5° of altitude angle as one data point, $C_{\mathrm{exp,EPR}}(\theta)$ and $C_{\mathrm{exp,COH}}(\theta)$, with $40^\circ < \theta < 60^\circ$.

We present the two-photon coincidence measurements between ground station and satellite (with noise subtracted) for data presented in Fig. 4 of the main text. There are five sets of data for 5 satellite passes in Table S1 and 4 sets of data for 4 satellite passes in Table S2. $C_{\mathrm{exp,EPR}}(\theta, i)$ ($C_{\mathrm{exp,COH}}(\theta, i)$) is the two-photon coincidence data with entangled (coherent) photon source for altitude angle between 40° and 60°. $C_{\mathrm{SQT,EPR}}(\theta, i)$ and $C_{\mathrm{SQT,COH}}(\theta, i)$ are calculated based on the standard quantum theory.

As described in the main text, the decoherence factor can be obtained as $D_{\mathrm{EPR}}(\theta, i) =$

$C_{\mathrm{exp,EPR}}(\theta, i)/C_{\mathrm{SQT,EPR}}(\theta, i)$, we take their average over different runs as $D_{\mathrm{EPR}}(\theta)$. We obtain similarly the factor $D_{\mathrm{COH}}(\theta)$ for the coherence source. The results are listed in Table S3.

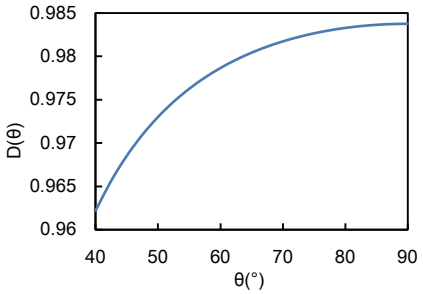

Fig. S1.
Decoherence factor as a function of altitude angle as predicted with Δ_t given by eq. (6). The coherence length of the photons is 0.07 mm and the satellite height is 500 km.

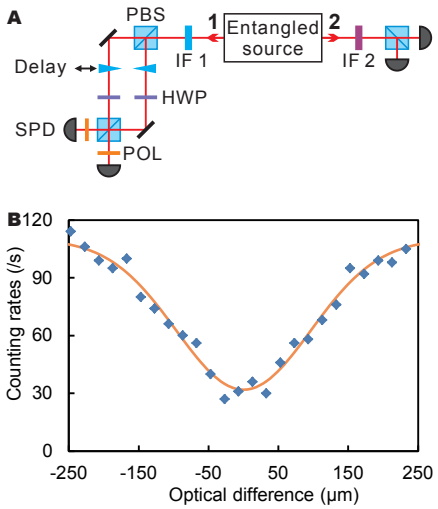

Fig. S2.
Hong-Ou-Mandel measurement with entangled photons produced in spontaneous parametric down conversion process (SPDC). (**A**) The detection of two photons in path 2 heralds the presence of a two-photon state in path 1. Both filters IF 1 and IF 2 are centered at 780 nm, with the bandwidths of 3 nm and 8 nm, respectively. (**B**) The simultaneous detection of two photons in path 1 and two photons in path 2 as a function of relative delay between the two arms of the interferometer in path 1 exhibits the Hong-Ou-Mandel dip. Scattered points: experimental data, solid line: fitting results with eq. (9).

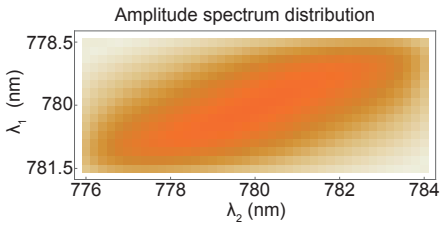

Fig. S3.
Two-photon joint spectrum of the SPDC process. The bandwidth of the used Gaussian filter is 3 nm for signal and 8 nm for idler photons.

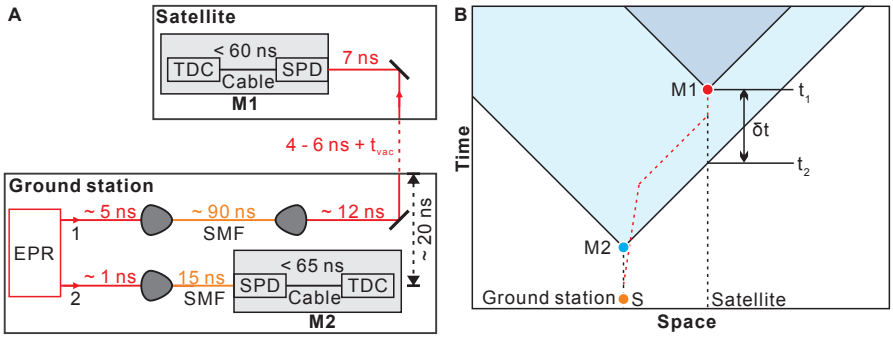

Fig. S4.
Spacetime analysis of entangled photon pairs. (**A**) presents the schematics for the latency incurred by photon creation and detection in the experiment. EPR: Einstein-Podolsky-Rosen photon-pair. (**B**) The corresponding spacetime analysis.

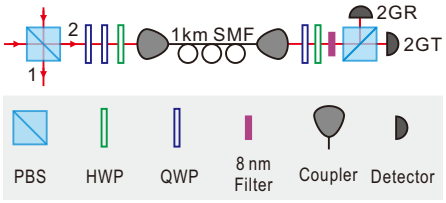

Fig. S5.
Experimental setup for adding 1 km fiber in path 2. A 1 km fiber is placed after the PBS separated photons 1 and 2. Two quarter-wave plates (QWPs) and one half-wave plate (HWP) before the coupler are used to compensate the photon polarization.

Table S1.
Measured two-photon coincidence events for coherent and entangled photon sources (for Fig. 4A in the main text).

		Satellite pass	$\theta(^\circ)$ 40 - 45	45 - 50	50 - 55	55 - 60
Coherent source	$C_{\mathrm{exp,COH}}(\theta, i)$	1	90	89	115	200
		2	64	83	62	72
		3	67	78	72	114
		4	65	120	–	–
		5	48	53	50	58
	$C_{\mathrm{SQT,COH}}(\theta, i)$	1	93	90	118	206
		2	69	87	66	76
		3	68	81	74	118
		4	68	123	–	–
		5	49	56	54	60
Entangled source	$C_{\mathrm{exp,EPR}}(\theta, i)$	1	103	88	139	240
		2	92	117	90	99
		3	85	130	79	136
		4	99	141	–	–
		5	50	74	65	58
	$C_{\mathrm{SQT,EPR}}(\theta, i)$	1	92	84	117	204
		2	76	127	91	115
		3	83	122	103	152
		4	126	158	–	–
		5	42	79	58	65

Table S2.
Measured two-photon coincidence events for coherent and entangled photon sources (for Fig. 4B in the main text).

		Satellite pass	$\theta(^\circ)$ 40 - 45	45 - 50	50 - 55	55 - 60
Coherent source	$C_{\mathrm{exp,COH}}(\theta, i)$	1	15	20	26	21
		2	15	18	28	–
		3	13	16	20	13
		4	21	29	65	23
	$C_{\mathrm{SQT,COH}}(\theta, i)$	1	17	22	27	24
		2	16	17	29	–
		3	14	19	23	15
		4	22	32	67	22
Entangled source	$C_{\mathrm{exp,EPR}}(\theta, i)$	1	22	34	24	31
		2	27	35	62	–
		3	20	30	28	18
		4	38	43	83	24
	$C_{\mathrm{SQT,EPR}}(\theta, i)$	1	23	31	33	28
		2	38	43	58	–
		3	18	26	35	24
		4	32	51	95	23

Table S3.
Decorrelation factors for the experiment.

$\theta(^\circ)$	D	Non-space-like		Space-like	
		D_{EPR}	D_{COH}	D_{EPR}	D_{COH}
40 – 45	9×10^{-12}	0.96 (7)	1.03 (13)	0.98 (13)	1.00 (12)
45 – 50	5×10^{-10}	0.97 (6)	0.97 (10)	0.93 (12)	0.98 (10)
50 – 55	8×10^{-9}	0.95 (6)	1.01 (11)	0.94 (9)	0.87 (7)
55 – 60	6×10^{-8}	0.96 (6)	0.96 (9)	0.92 (14)	0.96 (14)

References and Notes

1. S. Carlip, Quantum gravity: A progress report. *Rep. Prog. Phys.* **64**, 885–942 (2001). doi:10.1088/0034-4885/64/8/301

2. C. Kiefer, Quantum gravity: General introduction and recent developments. *Ann. Phys.* **15**, 129–148 (2005). doi:10.1002/andp.200510175

3. C. Rovelli, *Quantum Gravity* (Cambridge Univ. Press, 2004).

4. W. Marshall, C. Simon, R. Penrose, D. Bouwmeester, Towards quantum superpositions of a mirror. *Phys. Rev. Lett.* **91**, 130401 (2003). doi:10.1103/PhysRevLett.91.130401 Medline

5. I. Pikovski, M. R. Vanner, M. Aspelmeyer, M. S. Kim, C. Brukner, Probing Planck-scale physics with quantum optics. *Nat. Phys.* **8**, 393–397 (2012). doi:10.1038/nphys2262

6. H. Yang, H. Miao, D. S. Lee, B. Helou, Y. Chen, Macroscopic quantum mechanics in a classical spacetime. *Phys. Rev. Lett.* **110**, 170401 (2013). doi:10.1103/PhysRevLett.110.170401 Medline

7. A. Chou, H. Glass, H. R. Gustafson, C. Hogan, B. L. Kamai, O. Kwon, R. Lanza, L. McCuller, S. S. Meyer, J. Richardson, C. Stoughton, R. Tomlin, R. Weiss, The Holometer: an instrument to probe Planckian quantum geometry. *Class. Quantum Grav.* **34**, 065005 (2017).

8. A. Belenchia, R. M. Wald, F. Giacomini, E. Castro-Ruiz, Č. Brukner, M. Aspelmeyer, Quantum superposition of massive objects and the quantization of gravity. *Phys. Rev. D* **98**, 126009 (2018). doi:10.1103/PhysRevD.98.126009

9. D. Carney, P. C. E. Stamp, J. M. Taylor, Tabletop experiments for quantum gravity: a user's manual. *Class. Quantum Grav.* **36**, 034001 (2019).

10. H. Miao, D. Marytnov, H. Yang, Quantum correlation of light mediated by gravity. arXiv:1901.05827 [quant-ph] (17 January 2019).

11. T. C. Ralph, G. J. Milburn, T. Downes, Quantum connectivity of space-time and gravitationally induced decorrelation of entanglement. *Phys. Rev. A* **79**, 022121 (2009). doi:10.1103/PhysRevA.79.022121

12. T. C. Ralph, J. Pienaar, Entanglement decoherence in a gravitational well according to the event formalism. *New J. Phys.* **16**, 085008 (2014). doi:10.1088/1367-2630/16/8/085008

13. S. K. Joshi, J. Pienaar, T. C. Ralph, L. Cacciapuoti, W. McCutcheon, J. Rarity, D. Giggenbach, J. G. Lim, V. Makarov, I. Fuentes, T. Scheidl, E. Beckert, M. Bourennane, D. E. Bruschi, A. Cabello, J. Capmany, A. Carrasco-Casado, E. Diamanti, M. Dušek, D. Elser, A. Gulinatti, R. H. Hadfield, T. Jennewein, R. Kaltenbaek, M. A. Krainak, H.-K. Lo, C. Marquardt, G. Milburn, M. Peev, A. Poppe, V. Pruneri, R. Renner, C. Salomon, J. Skaar, N. Solomos, M. Stipčević, J. P. Torres, M. Toyoshima, P. Villoresi, I. Walmsley, G. Weihs, H. Weinfurter, A. Zeilinger, M. Żukowski, R. Ursin, Space quest mission proposal: Experimentally testing decoherence due to gravity. *New J. Phys.* **20**, 063016 (2018). doi:10.1088/1367-2630/aac58b

14. J. Friedman, M. S. Morris, I. D. Novikov, F. Echeverria, G. Klinkhammer, K. S. Thorne, U. Yurtsever, Cauchy problem in spacetimes with closed timelike curves. *Phys. Rev. D Part. Fields* **42**, 1915–1930 (1990). doi:10.1103/PhysRevD.42.1915 Medline

15. M. S. Morris, K. S. Thorne, Wormholes in spacetime and their use for interstellar travel: A tool for teaching general relativity. *Am. J. Phys.* **56**, 395–412 (1988). doi:10.1119/1.15620

16. H. D. Politzer, Simple quantum systems in spacetimes with closed timelike curves. *Phys. Rev. D Part. Fields* **46**, 4470–4476 (1992). doi:10.1103/PhysRevD.46.4470 Medline

17. D. Deutsch, Quantum mechanics near closed timelike lines. *Phys. Rev. D Part. Fields* **44**, 3197–3217 (1991). doi:10.1103/PhysRevD.44.3197 Medline

18. J. B. Hartle, Unitarity and causality in generalized quantum mechanics for nonchronal spacetimes. *Phys. Rev. D Part. Fields* **49**, 6543–6555 (1994). doi:10.1103/PhysRevD.49.6543 Medline

19. S. W. Hawking, Quantum coherence and closed timelike curves. *Phys. Rev. D Part. Fields* **52**, 5681–5686 (1995). doi:10.1103/PhysRevD.52.5681 Medline

20. F. Echeverria, G. Klinkhammer, K. S. Thorne, Billiard balls in wormhole spacetimes with closed timelike curves: Classical theory. *Phys. Rev. D Part. Fields* **44**, 1077–1099 (1991). doi:10.1103/PhysRevD.44.1077 Medline

21. H. D. Politzer, Path integrals, density matrices, and information flow with closed timelike curves. *Phys. Rev. D Part. Fields* **49**, 3981–3989 (1994). doi:10.1103/PhysRevD.49.3981 Medline

22. D. T. Pegg, *Quantum Mechanics and the Time Travel Paradox* (Consiglio Nazionale delle Richerche, 2001).

23. S. Lloyd, L. Maccone, R. Garcia-Patron, V. Giovannetti, Y. Shikano, S. Pirandola, L. A. Rozema, A. Darabi, Y. Soudagar, L. K. Shalm, A. M. Steinberg, Closed timelike curves via postselection: Theory and experimental test of consistency. *Phys. Rev. Lett.* **106**, 040403 (2011). doi:10.1103/PhysRevLett.106.040403 Medline

24. T. C. Ralph, T. G. Downes, Relativistic Quantum Information and Time Machines. *Contemp. Phys.* **53**, 1–16 (2012). doi:10.1080/00107514.2011.640146

25. J. L. Pienaar, C. R. Myers, T. C. Ralph, Quantum fields on closed timelike curves. *Phys. Rev. A* **84**, 062316 (2011). doi:10.1103/PhysRevA.84.062316

26. For more details, see supplementary materials.

27. J.-G. Ren, P. Xu, H.-L. Yong, L. Zhang, S.-K. Liao, J. Yin, W.-Y. Liu, W.-Q. Cai, M. Yang, L. Li, K.-X. Yang, X. Han, Y.-Q. Yao, J. Li, H.-Y. Wu, S. Wan, L. Liu, D.-Q. Liu, Y.-W. Kuang, Z.-P. He, P. Shang, C. Guo, R.-H. Zheng, K. Tian, Z.-C. Zhu, N.-L. Liu, C.-Y. Lu, R. Shu, Y.-A. Chen, C.-Z. Peng, J.-Y. Wang, J.-W. Pan, Ground-to-satellite quantum teleportation. *Nature* **549**, 70–73 (2017). doi:10.1038/nature23675 Medline

28. A. Kent, Causal quantum theory and the collapse locality loophole. *Phys. Rev. A* **72**, 012107 (2005). doi:10.1103/PhysRevA.72.012107

29. A. Kent, Nonlinearity without superluminality. *Phys. Rev. A* **72**, 012108 (2005). doi:10.1103/PhysRevA.72.012108

30. D. E. Bruschi, T. C. Ralph, I. Fuentes, T. Jennewein, M. Razavi, Spacetime effects on satellite-based quantum communications. *Phys. Rev. D Part. Fields Gravit. Cosmol.* **90**, 045041 (2014). doi:10.1103/PhysRevD.90.045041

31. D. Rideout, T. Jennewein, G. Amelino-Camelia, T. F. Demarie, B. L. Higgins, A. Kempf, A. Kent, R. Laflamme, X. Ma, R. B. Mann, E. Martín-Martínez, N. C. Menicucci, J. Moffat, C. Simon, R. Sorkin, L. Smolin, D. R. Terno, Fundamental quantum optics experiments conceivable with satellites – reaching relativistic distances and velocities. *Class. Quantum Gravity* **29**, 224011 (2012). doi:10.1088/0264-9381/29/22/224011

32. L.-K. Chen, Z.-D. Li, X.-C. Yao, M. Huang, W. Li, H. Lu, X. Yuan, Y.-B. Zhang, X. Jiang, C.-Z. Peng, L. Li, N.-L. Liu, X. Ma, C.-Y. Lu, Y.-A. Chen, J.-W. Pan, Observation of ten-photon entanglement using thin BiB_3O_6 crystals. *Optica* **4**, 77–83 (2017). doi:10.1364/OPTICA.4.000077

33. C. K. Law, I. A. Walmsley, J. H. Eberly, Continuous frequency entanglement: Effective finite hilbert space and entropy control. *Phys. Rev. Lett.* **84**, 5304–5307 (2000). doi:10.1103/PhysRevLett.84.5304 Medline

34. W. P. Grice, A. B. U'Ren, I. A. Walmsley, Eliminating frequency and space-time correlations in multiphoton states. *Phys. Rev. A* **64**, 063815 (2001). doi:10.1103/PhysRevA.64.063815

35. S.-K. Liao, W.-Q. Cai, W.-Y. Liu, L. Zhang, Y. Li, J.-G. Ren, J. Yin, Q. Shen, Y. Cao, Z.-P. Li, F.-Z. Li, X.-W. Chen, L.-H. Sun, J.-J. Jia, J.-C. Wu, X.-J. Jiang, J.-F. Wang, Y.-M. Huang, Q. Wang, Y.-L. Zhou, L. Deng, T. Xi, L. Ma, T. Hu, Q. Zhang, Y.-A. Chen, N.-L. Liu, X.-B. Wang, Z.-C. Zhu, C.-Y. Lu, R. Shu, C.-Z. Peng, J.-Y. Wang, J.-W. Pan, Satellite-to-ground quantum key distribution. *Nature* **549**, 43–47 (2017). doi:10.1038/nature23655 Medline

36. J. Yin, Y. Cao, Y.-H. Li, S.-K. Liao, L. Zhang, J.-G. Ren, W.-Q. Cai, W.-Y. Liu, B. Li, H. Dai, G.-B. Li, Q.-M. Lu, Y.-H. Gong, Y. Xu, S.-L. Li, F.-Z. Li, Y.-Y. Yin, Z.-Q. Jiang, M. Li, J.-J. Jia, G. Ren, D. He, Y.-L. Zhou, X.-X. Zhang, N. Wang, X. Chang, Z.-C. Zhu, N.-L. Liu, Y.-A. Chen, C.-Y. Lu, R. Shu, C.-Z. Peng, J.-Y. Wang, J.-W. Pan, Satellite-based entanglement distribution over 1200 kilometers. *Science* **356**, 1140–1144 (2017). doi:10.1126/science.aan3211 Medline

37. M. D. Eisaman, J. Fan, A. Migdall, S. V. Polyakov, Invited review article: Single-photon sources and detectors. *Rev. Sci. Instrum.* **82**, 071101 (2011). doi:10.1063/1.3610677 Medline